https://doi.org/10.46813/2024-154-067

INFLUENCE OF BOUNDARY CONDINIONS ON THE PLASMA POTENTIAL IN A HELICON DISCHARGE WITH PLANAR ANTENNA

V.F. Virko, Yu.V. Virko

Institute for Nuclear Research NAS of Ukraine, Kyiv, Ukraine

E-mail: y.v.virko@gmail.com

In a helicon discharge excited by a flat inductive antenna, situated at the discharge chamber end, distributions of plasma parameters have been measured by a thermo-emissive probe. The aim of the work was to define an influence producing by the bias potential of the surface being processed on plasma parameters in discharge chambers with either the dielectric or with conducting side walls. It was found that in the dielectric chamber application of a positive voltage and taking electron current to the surface under treatment causes increasing the plasma potential because the opposite sine current can not flow to the insulating wall. In the metal chamber increase of positive voltage on the surface leads to the discharge instability and break off for considerable taking electrons away from the discharge volume.

PACS: 52.80.-s

INTRODUCTION

For their high efficiency the helicon discharges are widely used in many applications [1]. The helicon waves are excited in magnetized plasma by inductive antennas of various types, most of which introduce electromagnetic energy to the discharge through the side boundary of plasma, perpendicularly to the external magnetic field lines [2, 3]. This requires using a discharge chamber with the dielectric side wall. Lately for excitation of the helicon discharges a so called "planar" antenna is often used, which represents a flat spiral situated behind a dielectric vacuum window at the discharge chamber end. [4]. In magnetic field this antenna also excites the azimuthally-symmetric mode $m = 0$ of helicon waves [5]. Unlike traditional helicon antennas the planar antenna supplies RF energy to the discharge along the magnetic field, in parallel to the axis that highly simplifies the design of technological equipment. By the way it makes unnecessary a separate discharge chamber and a treated surface may be placed directly opposite to the antenna, in the processing chamber with metal walls. Such a change in boundary conditions may have a significant influence on current distributions in the discharge and on the relation between a bias voltage, applied to the substrate, and the plasma potential. Since the mentioned parameters determine the energy of ions bombarding the substrate surface, they can also influence on the treatment process.

In the regimes typical for plasma technology the investigations of plasma parameters are complicated because high discharge power and particle density ($W \sim 1$ kW, $n \geq 10^{12}$ cm^{-3}). For this reason, the available information about plasma parameters in such discharges is not sufficient.

The common method for plasma potential measurement is application of thermo-emissive probes [6]. Usually, this probe represents a loop of tungsten wire which can be heated up to emission. The method is based on that the electron current may leave the probe only provided the probe potential is less (more negative) than the potential of surrounding plasma. The simplest way to use it consists in measuring the floating potential of the incandescent probe with a high impedance voltmeter. At sufficiently high emission this potential turns out to be close to the plasma potential. This method allows continuous recording and is the most convenient for studying the spatial distributions of plasma potential. But the emissive current density has to exceed a current density of plasma electrons coming to the probe at the plasma potential [7]. In considerably dense plasmas this requires heating the probe to a temperature close to the threshold of probe thermal stability.

A cold emissive probe may also be used as an ordinary Langmuir probe to estimate other plasma parameters, though its shape and effective pick-up area differ from those assumed in theory

1. EXPERIMENTAL SETUP

A schematic diagram of the experimental device is shown in Fig. 1,a. The quartz discharge chamber 1 of inner diameter 14 and 23 cm in length is placed in a longitudinal magnetic field created by coils 6. From one side the chamber is closed with a quartz window 2 of 12 mm thick, on the other side it is attached to a stainless-steel section 3 of the same diameter and 14 cm long. The inner surface of the quartz chamber may be covered with a conducting shield 4 of stainless tin, connected to the grounded section 3. In this case the discharge takes place in the chamber with conducting side walls.

The four-turn planar antenna 5 of an external diameter 11 cm and inner diameter 6.5 cm is placed close to the flat window 2. On the opposite side the discharge was terminated with the end plate electrode 7, which imitates a conducting substrate surface being processed. The inductive planar antenna 5 through a usual capacitive matching network was connected to an RF generator of frequency 13.56 MHz and 1 kW power.

Levels of incident and reflected power (the matching rate) were controlled by a directional coupler which was a part of the RF generator set. The most of measurements were made at a distance 30 cm from the antenna and 3.5 cm from the substrate electrode surface at Argon pressure 0.65 Pa in a magnetic field up to 6 mT.

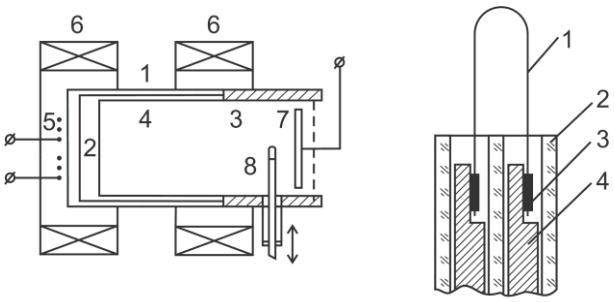

a *b*

Fig. 1. Scheme of the experimental device (a): 1 – quartz discharge chamber; 2 – quartz window; 3 – metal section; 4 – stainless shield; 5 – planar antenna; 6 – magnetic coils; 7 – the end plate electrode (the substrate); 8 – thermo-emissive probe. Emissive probe design(b) : 1 – tungsten filament 0.1 mm in diameter; 2 – ceramic tube of 3.2 mm diameter with two holes; 3 – gaskets of thin (50 μm) Ta foil; 4 – cupper wire 0.7 mm in diameter (b)

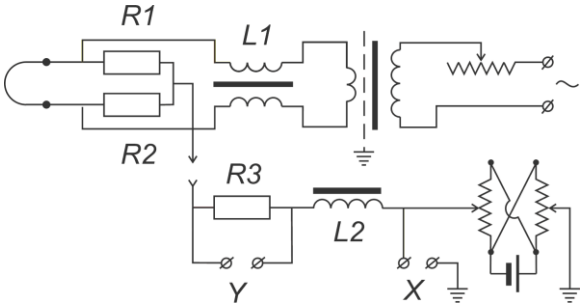

Fig. 2. Scheme of heating and measuring circuits of the emissive probe: R1 = R2 = 9 Ω; R3 = 10 Ω is the measuring resistor

The emissive probe 8 construction is shown in Fig. 1,b. The tungsten incandescent filament 1 was spot-welded to cupper holders 4 through the tantalum foil gaskets 3 and stuck from the ceramic insulation by 7 mm. The probe was inserted through a side port of the section 3 and could move along the diameter at a distance 3.5 cm from the end plate surface.

The scheme of the probe power supply and measuring circuits is depicted in Fig. 2. Two resistors $R1 = R2 = 9\ \Omega$ form the artificial middle point of the emitter. $R3 = 10\ \Omega$ is the measuring resistor. Terminals "X" and "Y" serve for connection the corresponding inputs of a two-coordinate recorder H-307. The inductive throttles *L1* and *L2* separated the probe from the heating circuits at high frequencies. For measuring radial distributions of the floating potential, the "Y"-input of the recorder, which had 1 MΩ impedance, was connected directly to the common point of resistors *R1* and *R2*, while to the "X"-input a signal proportional to the probe position was applied. In order to record the probe volt-ampere characteristics, the measuring resistor *R3* was connected to the probe middle point as is shown in the scheme.

2. RESULTS OF MEASUREMENTS

At the used argon pressure 0.65 Pa the discharge parameters depend on the generator output power *W*, the magnetic field B_0 and on matching conditions. As it was found, at insufficient RF power an increasing of magnetic field often leads to the discharge break up and cessation [5]. For this reason, the discharge was ignited at a low magnetic field $B_0 \le 1.2$ mT, after which the output power and the magnetic field simultaneously were increased up to their working magnitudes $W = 1$ kW, $B_0 = 6$ mT. At these conditions the discharge intensity was increasing and near the axis a blue light (of 2…3 cm in diameter) arose – because emission of the ionized argon spectral lines. This phenomenon is known as the "*blue core*" – regime. In this regime the average plasma density measured by an 8-mm interferometer in absence of the metal liner 4 was $n \sim 2 \cdot 10^{12}$ cm^{-3}.

At the fixed RF power 1 kW the plasma density in the measuring area essentially depends on the magnetic field strength. In Fig. 3 the radial distributions of ion saturation current I_i to the cold probe at probe voltage $U_p = -40$ V for three magnetic fields B_0 are shown: the curve 1 – $B_0 = 1.8$ mT, 2 – $B_0 = 3$ mT, and 3 – $B_0 = 6$ mT. Considering weak radial variations of the electron temperature T_e this current qualitatively represents the radial distribution of plasma density. From the figure it is seen that the magnetic field has an essential influence on both the density and the radial distribution of plasma coming to the treated surface.

As it was mentioned above the probe emission current that is necessary for its floating potential becomes close to the plasma potential, essentially depends on the plasma density. In Fig. 4 the dependencies of the probe potential, at which its current is equal to zero (that is of the floating potential U_{fl}) on the probe emission current I_e at the bias $U_p = -30$ V (that is on the degree of probe heating) are shown.

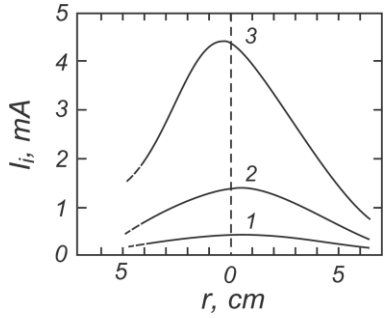

Fig. 3. Radial profiles of ion saturation current I_i to the cold probe: $U_p = -40$ V, $W = 1$ kW, $p = 0.65$ Pa. Magnetic fields: 1 – $B_0 = 1.8$ mT; 2 – $B_0 = 3$ mT; 3 – $B_0 = 6$ mT

These dependences have been obtained from the hot probe currant-voltage characteristics.

In Fig. 4,a the curve 1 was measured on the discharge axis ($r = 0$) in a magnetic field $B_0 = 2.4$ mT that corresponded to a moderate plasma density as is seen from the Fig. 3. The steady floating potential $U_{fl} \sim +(10…12)$ V, which apparently indicates the plasma potential φ_p is achieved at the emission current of $I_e \sim 25…$ 30 mA. On the contrary the curve 2 was obtained at the magnetic field $B_0 = 6$ mT at somewhat higher density and for this reason the stationary floating potential $U_{fl} \sim +6…7$ V settled down only at the higher emission current $I_e \sim 100$ mA. The emission current necessary for the potential saturation to occur is changing in the similar way when the density varies for any reason – because a radial displacement of the probe or because a change of discharge parameters.

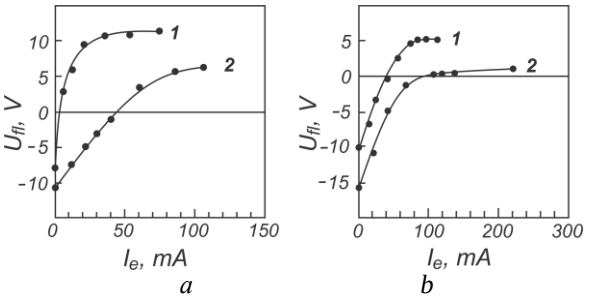

Fig. 4. Dependences of the probe floating potential U_{fl} on the emission current I_e at the bias voltage $U_p = -30$ V. $W = 1$ kW, $p = 0.65$ Pa, $r = 0$: a – the quartz discharge chamber, 1 – $B_0 = 2.4$ mT, 2 – $B_0 = 6$ mT; b – the magnetic field $B_0 = 6$ mT, 1 – the quartz chamber, 2 – the metal chamber. The end plate electrode (the substrate) was at a floating potential $U_{end} = –13$ V

Measurements in Fig. 4,a were made in the quartz discharge chamber at two magnetic fields. In Fig. 4,b the similar results were taken at the fixed magnetic field $B_0 = 6$ mT, but the curve 1 was obtained in the quartz chamber, while the curve 2 – in the chamber which side wall was covered by the grounded metal shield. As it is seen in the latter case (the curve 2 in Fig. 4,b) the emission current necessary for potential saturation remains rather high $I_e > 100$ mA, though the plasma potential in the metal chamber diminishes almost to zero.

The results in Fig. 4 were obtained when the end plate electrode was at a floating potential $U_{end} = -13$ V. The influence of a bias voltage applied to the plate U_{end} on the plasma potential is shown in Fig. 5. The measurements were made at three magnetic fields: the dashed lines – $B_0 = 1.8$ mT, dash-and-dotted lines – $B_0 = 3$ mT, lower solid lines – $B_0 = 6$ mT. The upper three curves 1 have been obtained at the maximal heating of the probe and correspond to the plasma potential φ_p. The lower three curves 2 in both figures represent the floating potential of the cold probe U_{fl} at the same magnetic fields. As it is seen from Fig. 5,a in the dielectric chamber the plasma potential φ_p grows roughly proportionally to the substrate-plate voltage U_{end} and achieves $\varphi_p \geq +40$ V. The floating potential of cold probe U_{fl} changes in the similar way. The difference $(\varphi_p - U_{fl}) \sim +(15...17)$ V is somewhat less than its theoretical value that for Argon gas at a typical electron temperature $T_e \sim 4$ eV has to be about $ln(M_i/m_e)^{1/2}T_e = 5.6\ T_e \sim 22.4$ V.

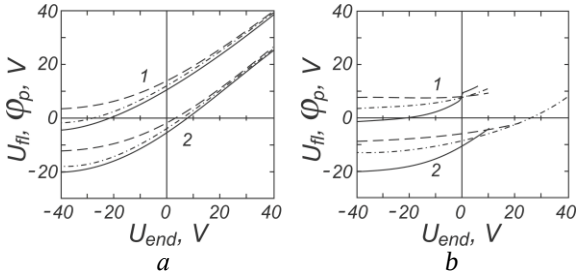

Fig. 5. Dependences of the floating potential of the hot emissive probe (upper curves 1, φ_p – is the plasma potential) and of the cold probe (lower curves 2, U_{fl}) against the bias potential of the end plate U_{end}: a – discharge in the dielectric chamber; b – discharge in the chamber with the conducting side wall. $W = 1$ kW, $p = 0.65$ Pa, $r = 0$. Magnetic fields: dashed curves – $B_0 = 1.8$ mT, dot-and-dash lines – $B_0 = 3$ mT, and the lower solid curves – $B_0 = 6$ mT

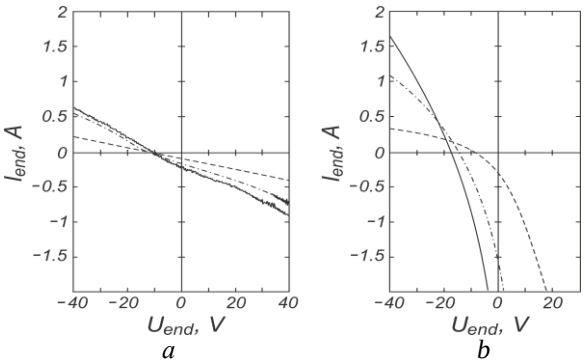

Fig. 6. Current to the end plate (to the substrate) I_{end} against its bias voltage U_{end}: a – in the dielectric discharge chamber; b – in the chamber with conducting wall. $W \approx 1$ kW, $p = 0.65$ Pa. Magnetic fields: the dashed curves – $B_0 = 1.8$ mT, dot-and-dash curves – $B_0 = 3$ mT, and the lower solid curves – $B_0 = 6$ mT

In the chamber which side wall is covered with the conducting shield 4 (see Fig. 5,b) at positive substrate voltages the discharge becomes unstable and when this voltage exceeds some critical value the discharge stops (breaks off). Before the discharge cessation the plasma potential amounts to $\varphi_p \leq +5…10$ V. The reason of such discharge behavior becomes clear from the volt-ampere characteristics of the substrate electrode which are shown in Fig. 6,a,b. As it is seen from Fig. 6,a in the dielectric chamber at positive voltages U_{end} of the end plate its electron current I_{end} is growing, but even at $U_{end} = +40$ V this current does not exceed $I_{end} = -1$ A. This limitation apparently is due to impossibility of compensation of the electron current to the end plate by a corresponding ion current to the dielectric wall. Such ion current from the plasma can to reach only an open surface of the metal section 3 (see Fig. 1,a), that has a small area. For this reason the current flow of both directions in the dielectric chamber meets a significantly high resistance.

On the contrary, in the metal chamber an ion current to the conducting wall is not limited and at positive

potentials of the end plate the electron current to it highly increases, as is shown in Fig. 6,b. In the magnetic field B_0 = 6 mT, that corresponds to rather high density (the solid down line), when the end plate voltage U_{end} approaches zero the electron current exceeds $I_e \geq$ -2 A and in our conditions it is limited by an available rectifier. The intensive taking the electrons away from the discharge volume leads at last to the discharge disruption and break-off.

The radial profiles of plasma potential in the quartz chamber at the generator output power $W \sim 1$ kW and at different values of magnetic field are shown in Fig. 7. The floating potential of strongly emitting probe, that is close to the plasma potential φ_p (the upper curves in Fig. 7), as well as the floating potential of cold probe U_{fl} (the lower curves) were measured.

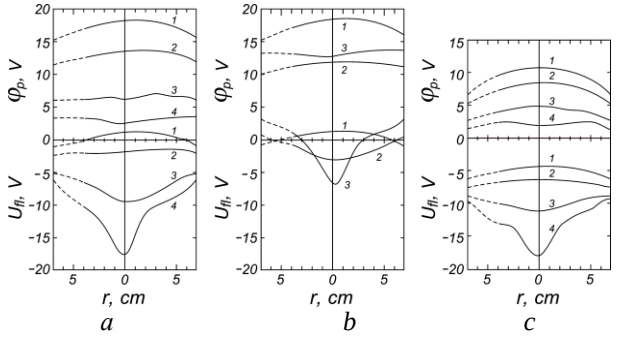

Fig. 7. Radial distributions of the plasma potential (upper curves φ_{pl}) and of the cold probe floating potential (lower curves U_{fl}); W = 1 kW: a – in the quartz discharge chamber; the end plate is under floating potential. Magnetic fields: 1 – B_0 = 0; 2 – 0.6 mT; 3 – 3 mT; 4 – 6.6 mT; b – the quartz chamber; the end plate is grounded U_{end} = 0: 1 – B_0 = 0.6 mT; 2 – 3 mT; 3 – 6 mT; c – the chamber with grounded metal side walls: 1 – B_0 = 0; 2 – 0.6 mT; 3 – 3 mT; 4 – 6 mT; connection of the plate to the ground has no impact on the potential distribution

Note, that when the magnetic field is reducing the plasma potential is growing and reaches $\varphi_p \sim +18$ V (the upper curve 1 in Fig. 7,a), while the plasma density significantly decreases. On the contrary at increasing magnetic field the density grows and at B_0 = 6…6.5 mT it attains $n \sim 2 \cdot 10^{12}$ cm^{-3}, but the plasma potential diminishes to a few volts (the upper curve 4 in Fig. 7,a).

At the same time the floating potential of the cold probe within the "blue core" acquires the most negative value $U_{fl} \sim -18$ V, that indicates the presence of electrons with enhanced energy in the near-axis region of the discharge (the lower curve 4 in Fig. 7,a).

The influence of the end plate voltage on the plasma potential in the dielectric chamber worth to be marked. At magnetic field B_0 = 6.6 mT the insulated end plate takes a floating potential of U_{end} = -13 V. When the end plate becomes grounded the electron current to it turns out to be 0.2 A, and the plasma potential, as well as the cold probe floating potential, increases by approximately +10 V as is shown with the upper and lower curves 3 in Fig. 7,b. On the contrary in the case when the quartz walls are covered with the grounded shield 4 (see Fig. 1), tough the floating potential of the end plate remains approximately the same, but its connection to the ground practically has no impact on the plasma potential. The corresponding profiles are shown in Fig. 7,c.

Using the cold emissive probe as a usual electrostatic probe radial distributions of the electron temperature were measured. Besides the possible errors for not adequate shape of the probe, in the RF discharges the probe characteristics may be distorted by potential oscillations which lead to exaggeration of the electron temperature [8]. To avoid this effect the so-called RF compensation of probes is used [9]. But in our experiments, despite the absence of compensation, the probe characteristics did not reveal an influence of potential oscillations, because their initial parts were fairy linear in a semi-logarithmic scale within two orders of the electron current magnitude.

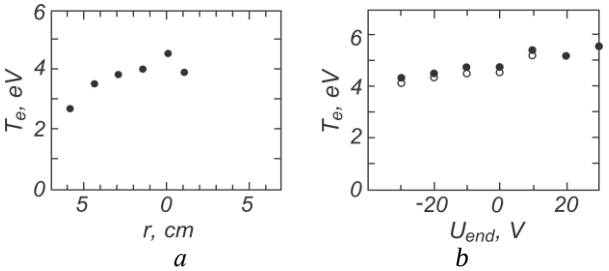

Fig. 8. Radial distribution of electron temperature T_e at discharge in the dielectric chamber with the grounded end plate electrode U_{end} = 0. The temperature distribution in the metal chamber is the same within errors of measurements (a). The electron temperature T_e on the discharge axis against the end plate voltage U_{end}. Black dots – discharge in the quartz chamber, light circles – in the metal chamber; W = 1 kW, B_0 = 6 mT, p = 0.65 Pa (b)

Moreover, the obtained temperatures do not exceed the typical values for the helicon discharges $T_e \sim$ 3…4 eV, that also indicates the absence of significant distortions for RF oscillations. A possible reason may be the presence in probe circuits the inductive coils (*L1* and *L2* in Fig. 2), that increases the probe impedance and, for some extend, contributes to probe compensation. At least we can suppose that obtained results correctly show the relative changes of temperature along the radius. The radial temperature profile T_e shown in Fig. 8,a have been measured in the dielectric chamber at W = 1 kW, B_0 = 6 mT and at grounded end plate U_{end} = 0. In the chamber with conducting wall the T_e distribution is the same within errors of measurements. Note a slight increase of the electron temperature near the discharge axis inside the "blue core", which visual diameter was about ~ 3 cm. This qualitatively agrees with a local increase of the floating potential on the axis as shown in Fig. 7.

The dependence of electron temperature T_e on the axis upon the end plate potential U_{end} is shown in Fig. 8,b. The light circles designate results obtained in the metal chamber. In this case at U_{end} = +10 V the electron current to the plate amounts to I_e = -2.5 A, and

at attempts to increase this voltage the discharge in the metal chamber breaks off. Unlike this in the dielectric chamber a positive voltage on the plate leads only to increase of the plasma potential, as is seen in Fig. 5,a, and to some rise of the electron temperature, that is shown by black dots in Fig. 8,b.

CONCLUSIONS

The radial profiles of the plasma potential in a helicon discharge excited by the planar antenna have been measured in discharge chambers with dielectric as well as with conducting side walls.

It has been confirmed that in a dielectric discharge chamber the ion current and the electron current to the surface under processing are restrained because they can not be closed by an opposite sign current to the wall. In this case the plasma potential grows with increasing the substrate potential.

In the chamber with conducting walls the ion current to the substrate is limited because difficult diffusion of electrons to the wall across magnetic field. Taking away an excessive electron current to the positively charged substrate causes the discharge instability and break off. Under increasing the magnetic field up to $B_0 = 6$ mT the density achieves $n \sim 2 \cdot 10^{12}$ cm^{-3} at $W = 1$ kW. Simultaneously the plasma potential, being approximately uniform along the radius, decreases to several volts. In this regime the floating potential of the cold probe on the axis amounts to ~ -20 V, and the electron temperature in the near axis region exceeds by about 1 eV the mean temperature over the discharge cross-section.

Note, that the results obtained in a model gas (Argon) can not be directly applied to discharges in technological media (molecular gases). The use of the "blue core" regime requires additional measures to improve the plasma uniformity.

REFERENCES

1. M.A. Liberman and A.J. Lichtenberg. *Principles of Plasma Discharges and Materials Processing*. New York: Wiley, 1994.
2. F.F. Chen. Physics of helicon discharges // *Phys. Plasmas*. 1996, v. 3, № 5, p.1783-1793.
3. F.F. Chen. Helicon discharges and sources: a review // *Plasma Sources Sci. Technol.* 2015, v. 24, № 1, p. 014001.
4. J.E. Stevens, V.J. Sowa, and J.L. Cecchi. Helicon plasma source excited by a flat spiral coil // *J. Vac. Sci. Technol. A*. 1995, v. 13, № 5, p. 2476-2482.
5. V.F. Virko, V.M. Slobodyan, K.P. Shamrai, Yu.V. Virko. Helicon Discharge excited by a Planar Antenna in bounded Volume // *Problems of Atomic Sci. Technol.* 2014, № 6, p. 130-136.
6. J.H. Sheehan and N. Hershkowitz. Emissive probes // *Plasma Sources Sci. Technol*. 2011, v. 20, № 6, p. 063001.
7. C. Cho, S. Kim, Y. Lee, I. Seong, W. Jeong, Y. You, M. Choi, and S. You. Determination of Plasma Potential Using an Emissive Probe with Floating Potential Method // *Materials.* 2023, v. 16, № 7, p. 2762.
8. F.F. Chen. Langmuir probe measurements in the intense RF field of a helicon discharge // *Plasma Sources Sci. Technol.* 2012, v. 21, № 5, p. 055013.
9. I. Sudit, F.F. Chen. RF compensated probes for high-density discharges // *Plasma Sources Science and Technology*. 1994, v. 3, № 2, p. 162.

Article received 30.09.2024

ВПЛИВ ГРАНИЧНИХ УМОВ НА ПОТЕНЦІАЛ ПЛАЗМИ ГЕЛІКОННОГО РОЗРЯДУ З ПЛАНАРНОЮ АНТЕНОЮ

В.Ф. Вірко, Ю.В. Вірко

У геліконному розряді, який збуджується плоскою індукційною антеною, розміщеною у торці розрядної камери, за допомогою термоемісійного зонда виміряні розподіли параметрів плазми. Метою роботи було з'ясування впливу потенціалу зміщення, прикладеного до оброблюваної поверхні, на параметри плазми у випадках розрядної камери з діелектричною або ж з провідною бічною стінкою. Встановлено, що у діелектричній розрядній камері прикладання позитивної напруги і відбір електронного струму на оброблювану поверхню спричиняє підвищення потенціалу плазми, оскільки струм протилежної полярності не може протікати на ізолюючу бічну стінку. У металевій камері збільшення позитивної напруги на оброблюваній поверхні веде до нестійкості розряду і його зриву через значний відбір електронів з розрядного об'єму.